Free Space Optical Multicast Crossbar

Abdelbaset S. Hamza, Jitender S. Deogun, and Dennis R. Alexander

***Abstract*—Enabling multicast in optical networks requires the use of multicast-capable optical switches. In this paper, we propose a new class of multicast-capable free space optical (FSO) switches. Our design exploits nonmovable tri-state switching elements (T-SEs) that support signal splitting and switching simultaneously and seamlessly, and thus the separate splitting stages used in conventional multicast switches are not needed. It follows that the propagation loss that may be encountered by an optical beam passing through a splitting stage followed by a crossbar (e.g., splitter-and-delivery-based switches) can be avoided in the proposed switch since the beam passes only through the crossbar. The proposed FSO switch is analyzed and compared to conventional architectures in terms of hardware complexity, power loss, and cost. We show that an $N \times M$ switch requires only NM nonmovable T-SEs. Comparison with existing optical multicast switches shows that the proposed switch provides multicast capability with substantially lower hardware complexity and a comparable performance. Cost analysis for the proposed switch shows that its switching cost is lower than existing switches even if the cost of the T-SE is 1.2 to 2.2× that of a MEMS mirror.**

***Index Terms*—Free Space Optical; MEMS; Multicast; Optical Switching; Switching.**

I. Introduction

A data center (DC) design paradigm has been evolving to facilitate the development of mega DCs that support 100,000 servers and beyond [1]. The demand for mega DCs has been increasing as the portfolio of bandwidth- and computation-intensive Big Data applications continues to grow [2,3]. Examples of Big Data applications can be found in disciplines such as social media, bioinformatics, the Internet-of-Things, nanoinformatics, and real-time research analytic services. Applications hosted by mega DCs generate large demands for bandwidth with different communication patterns involving a combination of unicast, multicast, in-cast, and all-to-all-cast traffic [1,4]. For example, Hadoop and Spark frameworks require in-cast traffic delivery during the shuffle stage of MapReduce but need multicast for data replication, parallel database joint operations, as well as data dissemination in virtual machine provisioning [4].

Manuscript received June 9, 2015; revised September 18, 2015; accepted November 2, 2015; published December 10, 2015 (Doc. ID 241663).

A. S. Hamza (e-mail: ahamza@cse.unl.edu) and J. S. Deogun are with the Department of Computer Science and Computer Engineering (CSE), University of Nebraska-Lincoln, Lincoln, Nebraska 68588-0115, USA.

A.S. Hamza and D. R. Alexander are with the Department of Electrical and Computer Engineering (ECE), University of Nebraska-Lincoln, Lincoln, Nebraska 68588-0511, USA.

http://dx.doi.org/10.1364/JOCN.8.000001

Optical technologies have become an integral part of today's communication networks. The inherent high bandwidth of optical networks makes them capable of meeting the high-speed, high-bandwidth requirements projected by mega DC applications and services. Therefore, DC architectures using optical interconnects to realize optical circuit switching or optical burst switching on top of electrical packet switching have been recently proposed [4–7]. On the other hand, different research proposals investigate the feasibility of realizing all-optical DC interconnects [8–12]. Optical technologies have been long seen as a viable solution for not only providing high bandwidth [13–15] but also implementing multicasting more efficiently compared to higher layer implementations (e.g., the application layer). Realizing multicast in the optical layer requires the development of efficient multicast-capable optical switches.

Optical switches can be generally implemented either in guided space (using waveguides) or free space [using free space optical (FSO) switches]. Guided technologies, such as array waveguide grating routers (AWGRs) with tunable wavelength converters or tunable lasers, and semiconductor optical amplifiers (SOAs) can be used to realize fast optical switches with switching time in the range of a few nanoseconds. However, switches based on AWGRs and SOAs are usually expensive [16]. On the other hand, FSO switches have low insertion loss and crosstalk and simple fabrication, are less expensive and data-rate independent, and support bidirectional communication [15,16]. However, FSO switches are slower than guided switches, and the switching time is in the range of tens of milliseconds. A common approach for developing FSO switches is to use 2D/3D micro-electro-mechanical systems (MEMS) [15]. MEMS designs use movable mirrors to direct beams from inputs to outputs, which may lead to losses due to angular misalignments. Another approach to develop FSO switches is to use electro-optic and liquid crystal materials [15,17], where an electric field is used to configure switching elements (SEs) into either transmissive or reflective states.

Real world DC traffic traces show that more than 95% of the data are being transferred by the top 10% largest elephant flows (i.e., flows with large amounts of data) [18]. Researchers are currently investigating DC optical interconnects using hybrid optical switching schemes in which fast and slow optical switches are used simultaneously [9,11,16,19]. Fast optical switches are used for packets and small bursts of data, whereas slow optical switches are used for long-lived (circuit and long burst) traffic. Therefore, there is a current practical need for slow yet efficient and cheap multicast optical switches.

1943-0620/16/010001-10$15.00/0

Most existing FSO designs are for unicast [15] transmissions, and hence incorporating multicast into these switches requires additional hardware (e.g., splitters). This results in a higher complexity and thus cost. Moreover, the existence of a splitting stage adds to the overall basic switching structure and thus can potentially add to the overall loss experienced by the signal due to Gaussian beam divergence. Accordingly, the design of multicast FSO switches with reduced complexity and path lengths is an interesting yet challenging problem. To this end, we propose a new $N \times M$ strictly nonblocking (SNB) multicast FSO switch using only NM nonmovable tri-state SEs (T-SEs). Compared to existing multicast optical switches, the new switch is shown to exhibit a substantial reduction in hardware complexity and path lengths and has a reduced cost.

The remainder of the paper is organized as follows. In Section II, we review and analyze existing FSO multicast switches. We dedicate Section III to presenting the new class of FSO multicast switches. Results are presented in Section IV, followed by a discussion in Section V. Conclusions are presented in Section VI.

II. Related Work and Preliminaries

In this section, we introduce notations and definitions and review existing FSO switches.

A. Notation

An $N \times M$ switch has N input ports; $\mathcal{I} = \{I_0, \ldots, I_{N-1}\}$ has M output ports; and $\Omega = \{O_0, \ldots, O_{M-1}\}$. A connection request between an input port I_p, $1 \le p \le N$, and an ordered set of output port(s) Ω_p, $\Omega_p \subseteq \Omega$, is denoted by $\mathcal{R}_p = \langle I_p, \Omega_p \rangle$. A request $\mathcal{R}_p$ is said to be a multicast if $1 < |\Omega_p| < N$, a unicast if $|\Omega_p| = 1$, or a broadcast if $|\Omega_p| = M$ (i.e., $\Omega_p = \Omega$). A set of all requests in an $N \times M$ switch $\mathcal{R}^{N \times M}$ can be any combination of unicast requests Γ, $1 \le |\Gamma| \le \min(N, M)$, and multicast requests Ψ, $1 \le |\Psi| \le \min(N, \lfloor M/2 \rfloor)$.

B. MEMS-Based FSO Multicast Switches

Several multicast optical switch architectures have been investigated in the literature (e.g., [14,20,21]). Optical splitter and delivery (SaD) is a well-known SNB multicast switch [20]. Figure 1(a) shows an $N \times N$ SaD switch where each input beam is initially split to N identical branches using a $1 \times N$ splitter. Corresponding branches from all N splitters are connected to one output port. Thus, any input can be connected to any number of output ports. It is worth noting that the SaD switch does not distinguish between unicast and multicast requests, which results in unnecessary splitting and signal losses. To overcome unnecessary splitting, configurable splitters may be used that add to the complexity of the design and control of the switch [21].

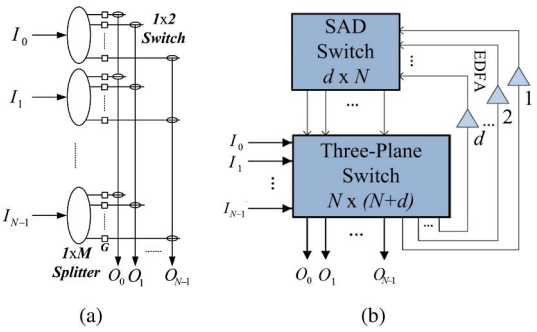

Fig. 1. $N \times N$ switch. (a) SaD [20] and (b) SUM-SaD [13].

A MEMS-based multicast FSO switch can be implemented using SaD architecture (SaD-I) [20] by replacing the 1×2 switches with MEMS mirrors. In Fig. 2(a), we propose a possible realization of a 1×4 FSO splitter. The total number of components used in a $1 \times N$ splitter is $\Phi = 2^{\lceil \log_2(N) \rceil + 1} - 2$.

SaD-I can be further improved by employing configurable splitters (SaD-II) [21]. Figure 2(b) shows a possible realization of a configurable 1×4 splitter. The total number of components used in a $1 \times N$ configurable splitter is 2Φ. In SaD-II switches, each input beam is divided into a number of beams equal to the cardinality of the output set ($|\Omega_p|$), eliminating unnecessary splitting [21]. It can be seen that SaD-II behaves like 2D MEMS and SaD-I in the cases of unicast and broadcast, respectively.

A switch that treats unicast and multicast requests separately is proposed in [13,14]. The architecture combines a $d \times N$ SaD switch and an $N \times (N + d)$ three-plane switch [Fig. 1(b)] to realize an SNB switch (SUM-SaD). Unicast requests are switched by the three-plane switch, and only multicast requests are delivered by the SaD. Thus, splitting loss for unicast and multicast is similar to that of SaD-II and SaD-I, respectively.

In [22], Lin *et al.* propose an FSO 2D MEMS switch that performs bridging to restore failed links. Bridging can be thought of as a special case of multicast where an input signal is forwarded to exactly two outputs.

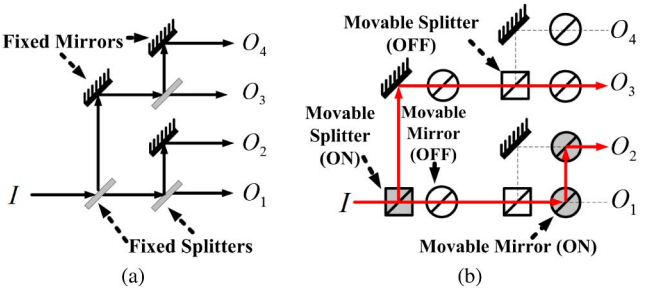

Fig. 2. Possible realization of 1×4 FSO splitter. (a) Conventional and (b) configurable.

III. Proposed Multicast FSO Switch Design

We propose a new class of SNB multicast FSO crossbar switches using T-SEs. A T-SE is placed at every node, i.e., row–column intersection. SE(p,q) denotes a T-SE at the intersection of input port p and output port q, $(1 \le p \le N$ and $1 \le q \le M)$.

A T-SE can be configured (see Fig. 3) in one of three states: reflective (R); transmissive (T); or splitting (S), half reflective/half transmissive [23,24]. The configuration of SE(p,q) is denoted by $\tau(p,q,\chi)$, where $\chi \in \{R,T,S\}$ represents the state of the T-SE. It is assumed that all T-SEs are initially in the T-state.

Figure 4(a) shows the four possible configurations of the basic 2×2 switch where the S-state is used to perform the required multicasting. Figure 4(b) depicts a 5×5 switch with two multicast requests: $\langle 1,\{1,3,4\}\rangle$ and $\langle 4,\{0,2\}\rangle$. The request $\langle 1,\{1,3,4\}\rangle$ is realized using the following T-SE configurations: $\tau(1,1,S)$, $\tau(1,3,S)$, and $\tau(1,4,R)$.

A. Switch Properties

In the following, we analyze the proposed switch with respect to hardware complexity, signal path length, and number of T-SEs in the S-state.

Hardware complexity. In the proposed switch, signal splitting and switching are performed simultaneously and seamlessly. Therefore, the proposed design supports multicast without a separate splitting stage and thus has lower complexity.

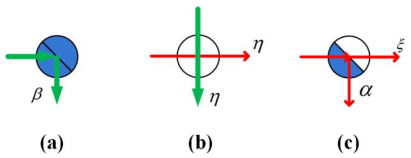

Fig. 3. T-SE. (a) R-state, (b) T-state, and (c) S-state.

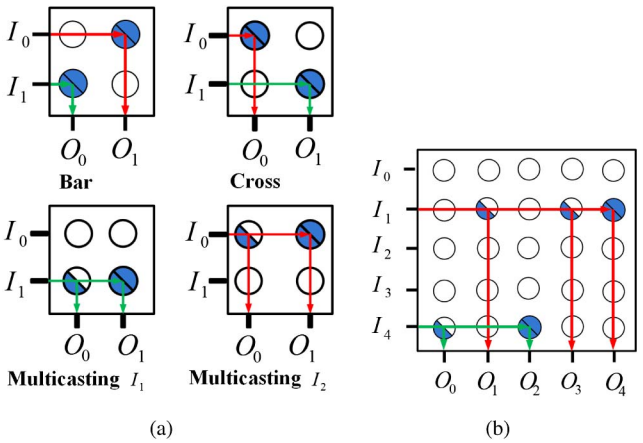

Fig. 4. (a) Switching modes in a 2×2 switch and (b) multicast in a 4×4 switch.

Signal path length. The performance of the proposed switch depends on the number of T-SEs traversed by the light beam and the number of splitting operations. For an $N \times M$ switch, the number of T-SEs in the shortest and longest signal paths are 1 and $(N + M - 1)$, respectively.

Lemma 1. *The minimum and maximum number of T-SEs configured in an S-state are 1 and $M-1$, respectively.*

Proof. This directly follows from the minimum and maximum cardinalities of multicast connections, which are 2 and M including the broadcast case, respectively. □

Lemma 2. *For all requests at a given time, the total number of T-SEs configured in the S-state is given by $M_\Psi - |\Psi|$, where $2 \le M_\Psi \le M$ is the number of output ports in all multicast requests at that time $M_\Psi = \sum_{w=1}^{|\Psi|} \Omega_w, \forall\, \mathcal{R}_p \in \Psi$.*

Proof. For each multicast request $\langle I_p, \Omega_p\rangle$, all T-SEs in the row corresponding to the input port and columns corresponding to output ports in Ω_p are configured in the S-state except for the last output port in Ω_p, which is configured in the R-state. Therefore, the total number of T-SEs in the R-state out of M_Ψ is equal to the total number of multicast requests $|\Psi|$. □

In the remainder of the paper, we assume that $M = N$. The analysis and results can be easily extended to the case of $M \ne N$.

Theorem 1. *An $N \times N$ crossbar switch employing T-SEs is strictly a nonblocking multicast switch.*

Theorem 1 can be proved using induction. The complete proof is discussed in Appendix A.

Given that the proposed switch is SNB, it follows that the configuration (routing) of a connection request $\mathcal{R}_p = \langle I_p, \Omega_p\rangle$ on the proposed switch is straightforward and can be realized by configuring the corresponding T-SEs in S- and/or R-states as required.

B. Signal Power Loss

An optical signal undergoes losses as it propagates from input to output ports in an FSO switch. There are two types of losses: insertion/coupling and splitting losses.

Insertion and Coupling Losses. This is mainly due to the Gaussian beam divergence experienced by any beam propagating in free space [25]. Extensive analysis and studies have been performed to characterize the performance of 2D MEMS with respect to the insertion and coupling losses. These losses in our design follow the analysis used for MEMS switches [25] but with the following two differences:

1) In MEMS-based multicast switches, an optical beam must propagate through a splitting stage before being switched by a crossbar. However, in the proposed switch, an optical beam propagates only through a crossbar in which splitting and switching are performed simultaneously and seamlessly. This can reduce the insertion loss due to Gaussian beam divergence.

2) In MEMS, mechanical motion of the mirrors results in angular misalignment, leading to inefficient coupling. The proposed design, however, employs only nonmovable parts and is free of such losses.

Splitting Losses. Splitting losses are the losses encountered by the light beam due to the splitting required for multicasting. In SaD-based switches, an input beam is split using a $1 \times N$ splitter into N and $|\Omega_p|$ equal signals in conventional and configurable splitters, respectively. Following the splitting stage, a beam travels in free space from the input to output ports in a crossbar reflecting off of a single mirror.

In the proposed design, the beam may incur losses due to the cascaded splitting nature of the crossbar as it propagates through a chain of nonmovable T-SEs along its path to the output. Let β and η be the reflection and transmission efficiencies of T-SE in the R- and T- states, respectively. We refer to the percentage of the power reflected by a T-SE in the S-state as α, and the transmitted power of the beam is ζ (Fig. 3). In our proposed switch, splitting losses depend on the cardinality of the output set $|\Omega_p|$, and thus we have two cases.

Case 1: Unicast ($|W_p| = 1$). Power loss is due to the reflection from SE$(p, O^p_{q,1})$, transmission losses of the $(N-1-p)$ T-SEs before the reflection, and transmission losses of the q T-SEs after the reflection. The loss in the unicast case $[L_{\text{UC}}(I_p, O^p_{q,1})]$ is given by

$$L_{\text{UC}}(I_p, O^p_{q,1}) = 10\log_{10}(\beta \cdot \eta^{N-1-p+q}). \tag{1}$$

The lower (upper) bounds for L_{UC} are related to the shortest (longest) path traversed by the light beam

$$10\log_{10}(\beta) \le L_{\text{UC}} \le 10\log_{10}(\eta^{2(N-1)} \cdot \beta). \tag{2}$$

Case 2: Multicast ($1 < |\Omega_p| < M$). The optical losses of an output $O^p_{q,k} \in \Omega_p$ are due to the transmission losses of $(N-p+q-k)$ T-SEs in the T-state, transmission losses of $k-1$ T-SEs in the S-state, and the reflection loss of a T-SE in the S- or R-states. The losses in the multicast case $L_{\text{MC}}(I_p, O^p_{q,k})$ are given by

$$L_{\text{MC}}(I_p, O^p_{q,k}) = 10\log_{10}((\sigma \cdot \alpha + (1-\sigma) \cdot \beta) \cdot \eta^{N-p+q-k} \cdot \zeta^{k-1}), \tag{3}$$

where $\sigma = 1$ for $1 \le k < |\Omega_p|$ and $\sigma = 0$ for $k = |\Omega_p|$. Using Lemmas 1 and 2, the lower (upper) bounds for losses in multicast requests are given by

$$10\log_{10}(\alpha) \le L_{\text{MC}} \le 10\log_{10}(\beta \cdot (\eta \cdot \zeta)^{N-1}). \tag{4}$$

The equations for the broadcast case (i.e., $|\Omega_p| = N$) can be easily deduced from Eq. (3) and inequality (4) by setting $|\Psi| = 1$ and $M_\Psi = N$.

IV. Results and Analysis

Two-dimensional FSO crossbars are generally of low scalability due to Gaussian beam propagation loss, which becomes the dominant source of losses at high-port count [26]. Therefore, in this section, we present a comparative analysis of the proposed switch with respect to hardware complexity, power splitting, and cost for $N = 8$ (i.e., 8×8 switches).

A. Hardware Complexity

We decompose all switches into five basic elements, namely: fixed/movable mirrors, fixed/movable splitting mirrors, and T-SEs. Table I summarizes the hardware complexity of architectures under consideration. Figure 5 depicts the hardware complexity for $N = 8$.

In SaD-I, all requests including unicast undergo $1 \times N$ splitting. Therefore, no extra hardware is needed to separate unicast connections, leading to a lower hardware complexity for SaD-I. SaD-II is similar to SaD-I except that configurable splitters are used to separate unicast and multicast connections. Even for multicast connections, SaD-II is capable of splitting the input beam to the exact size of the output set. However, this comes at the expense of additional hardware and control complexity. SUM-SaD separates unicast and multicast connections and has lower hardware complexity as compared to that of SaD-II. The hardware complexity of SUM-SaD is comparable to that of SaD-I, although SUM-SaD uses more movable components. On the other hand, the proposed crossbar switch using T-SEs is capable of separating the unicast and multicast connections using a smaller number of hardware components (i.e., N^2) as compared to SaD-based switches.

B. Power Splitting Properties

To evaluate the performance of the proposed switch, we calculate the power penalties of the four architectures of size 8×8. We calculate the losses at the eight output ports for all 255 possible combinations of different output set sizes. Since the splitting loss in the proposed switch

TABLE I
Summary of Hardware Complexity of Different Architectures $\Phi = (2^{(\lceil \log_2(N) \rceil + 1)} - 2)$

	Movable Mirror	Fixed Mirror	Movable Splitter	Fixed Splitter	T-SE
SaD-I	N^2	$N\Phi/2$	—	$N\Phi/2$	—
SaD-II	$N^2 + N\Phi$	$N\Phi/2$	$N\Phi/2$	—	—
SUM-SaD	$2N^2$	$N\Phi/4$	—	$N\Phi/4$	—
Proposed	—	—	—	—	N^2

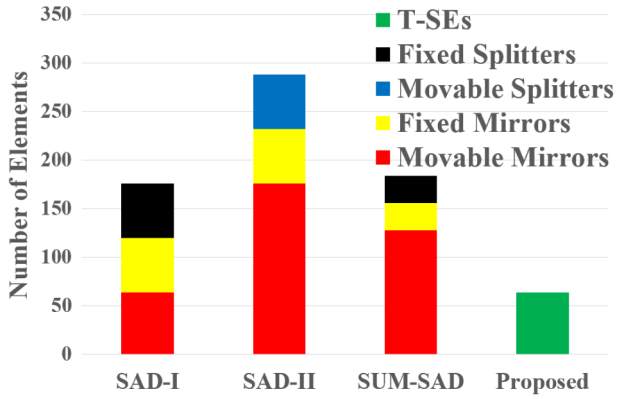

Fig. 5. Hardware complexity for an 8 × 8 switch.

depends on the input port, we calculate the signal loss for the first and eighth input ports to represent the lower and upper bounds of the splitting loss, respectively.

We use the commercial specifications reported by Kent Optronics [27] for the tri-state material e-TransFlector, which can be tuned to operate in the IR spectrum range used by existing optical communication networks. For example, Hamedazimi *et al.* [28] demonstrated a proof-of-concept of an FSO communication link for DC communication using the e-TransFlector material tuned for the IR spectrum. Accordingly, we set both reflectance in R-state (β) and transmittance in T-state (η) to 87%, whereas for the S-state, both transmittance (ζ) and reflectance (α) are set to 43%. We assume that the optical efficiency of all fixed/movable mirrors and splitters are 99% and 49%, respectively [29].

In the case of SaD-I, the power loss is independent of the output set size and is given by

$$L_{\text{SaDI}} = 10\log_{10}(0.99) + 10\log_{10}(1/N). \tag{5}$$

For SaD-II, the unnecessary splitting is avoided, and thus splitting loss depends on $|\Omega_p|$ given by

$$L_{\text{SaDII}} = 10\log_{10}(0.99) + 10\log_{10}(1/|\Omega_p|). \tag{6}$$

Figures 6(a)–6(c) depict the average minimum, average, and average maximum splitting power losses of the four switch architectures under consideration at different sizes of output sets.

In the unicast case, SaD-II and SUM-SaD have the same performance. This performance is better than other architectures (see Fig. 6) because the unicast connections are switched separately without incurring any additional losses. On the other hand, SaD-I has the highest power penalty (~9.3 dB) due to the fact that unicast connections undergo unnecessary forced power splitting. Although the proposed architecture does not enforce splitting for unicast connections, there are additional losses of 4.53 dB and 7 dB for input ports 1 and 8, respectively. This is due to the propagation of the beam through the nonmovable T-SEs configured in the T-state along its path. Even though this

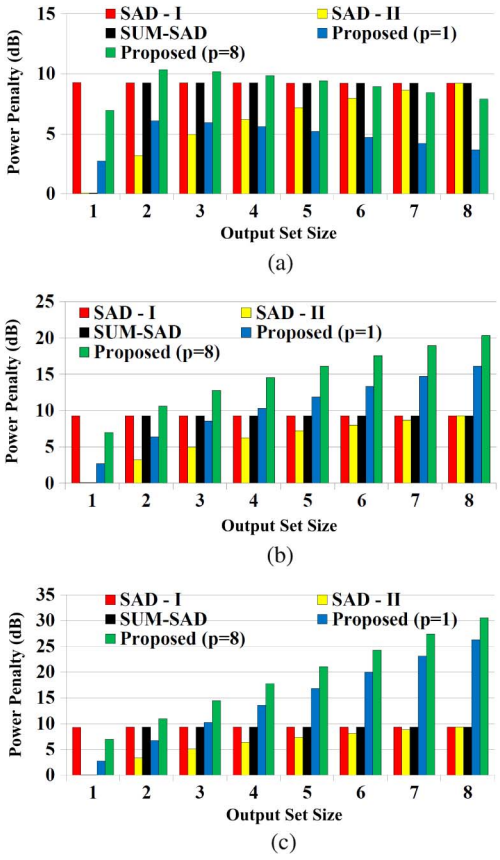

Fig. 6. Splitting power penalty in an 8 × 8 switch. (a) Minimum, (b) average, and (c) maximum.

does not split the beam, it adds additional losses due to the imperfection of the material.

In the multicast case (i.e., starting from an output set size of two), it can be observed that as the size of the output set increases, so does the average and average maximum power penalties in all architectures except for SaD-I and SUM-SaD that have a fixed power loss (~9.3 dB). This is because SaD-I and SUM-SaD perform fixed full splitting for all input signals regardless of the size of the output set.

The average minimum power loss in the case of SaD-II also increases as the size of the output set increases, whereas the average minimum loss is fixed for SaD-I and SUM-SaD due to the full splitting property. The average minimum losses in the proposed switch monotonically decrease starting with the output size of two. However, we observe an increase in the average minimum losses from an output size of one to an output size of two.

Average minimum (maximum) losses depend on the number of combinations at different sizes of output sets. This number increases starting from an output set size of one (i.e., eight possible combinations of unicast) to four (i.e., 70 possible combinations) and then decreases.

Regardless of the decrease in the number of combinations starting from an output set size of four, average maximum loss experiences a monotonic increase as the aggregated maximum loss becomes dominant, whereas the

average minimum loss decreases as the size of the output set increases.

The proposed switch outperforms both SaD-I and SUM-SaD up to an output size of two, whereas its performance is comparable to the other architectures up to an output set size of four, after which the power loss increases.

It is worth pointing that we only consider the splitting losses in our analysis. Although MEMS-based switches show relatively lower splitting power losses, MEMS-based switches incur additional losses because of the Gaussian beam losses due to the propagation of the beam in the separate splitting stage and the angular misalignment of the micro-mirrors [22,25]. Losses due to angular misalignment can become more significant if the light beam experiences multiple reflections such as in $1 \times N$ beam splitters [30,31].

High power losses can cause the signal power to fall below the sensitivity of the optical receiver, and thus amplification at the input ports may be needed. It might also be noted that the proposed switch experiences variation in the splitting power losses at output ports. For example, in the case of an output set size of eight, the variation between the minimum and maximum splitting loss is 25 dB (see Fig. 6). In order to alleviate the impact of the varying power loss at the outputs, variable optical attenuators (VOAs) must be used at the output ports to equalize the impact of the insertion loss so that the power of the received signal falls within the dynamic range of the optical receiver [32].

Even though MEMS-based switches do not demonstrate differences between minimum and maximum splitting power losses at the output ports as compared to the proposed switch, MEMS-based switches still need pre-amplifiers, e.g., SUM-SaD [see Fig. 1(b)], and variable optical attenuators due to the losses encountered by the signal in the splitting stage.

Table II summarizes the number of amplifiers and VOAs required by the switches investigated. The proposed switch, SaD-I, and SaD-II need N amplifiers and N VOAs. However, SUM-SaD switches require N VOAs and $N/2$ amplifiers. This is because only $N/2$ of the inputs are propagating through the splitting stage, as shown in Fig. 1(b).

C. Switch Cost Analysis

From the discussion above, the total cost ($C_{\text{tot}}^{\text{arch}}$) of a switch architecture *arch* depends on the costs of VOAs ($C_{\text{VOA}}^{\text{arch}}$), amplifiers ($C_{\text{amp}}^{\text{arch}}$), and switching elements ($C_{\text{sw}}^{\text{arch}}$) used, and is given by

TABLE II
NUMBER OF AMPLIFIERS AND VOAS

	Amplifiers	VOAs
SaD-I	N	N
SaD-II	N	N
SUM-SaD	$N/2$	N
Proposed	N	N

$$C_{\text{tot}}^{\text{arch}} = C_{\text{VOA}}^{\text{arch}} + C_{\text{amp}}^{\text{arch}} + C_{\text{sw}}^{\text{arch}}, \tag{7}$$

where *arch* can be SaD-I, SaD-II, SUM-SaD, or the proposed switch. $C_{\text{VOA}}^{\text{arch}}$ and $C_{\text{amp}}^{\text{arch}}$ depend on the number of VOAs ($N_{\text{VOA}}^{\text{arch}}$) and amplifiers ($N_{\text{amp}}^{\text{arch}}$) used, respectively.

From Table II, SaD-I, SaD-II, and the proposed switch architectures employ N VOAs at the output ports and N amplifiers at the input ports. However, SUM-SaD switch architecture requires N VOAs and only $N/2$ amplifiers. Therefore, SUM-SaD architecture has a cost advantage over SaD-I, SaD-II, and the proposed architecture with respect to C_{amp}.

We can expand $C_{\text{sw}}^{\text{arch}}$ further and express it as a function of the cost of a fixed (mirror/splitter) component C_f, a movable (mirror/splitter) component C_m, and a T-SE C_{tse}. Given the cost of each component, we can use Table I to calculate $C_{\text{sw}}^{\text{arch}}$ as follows:

$$C_{\text{sw}}^{\text{arch}} = N_f^{\text{arch}} \cdot C_f + N_m^{\text{arch}} \cdot C_m + N_{\text{tse}}^{\text{arch}} \cdot C_{\text{tse}}, \tag{8}$$

where $N_f^{\text{arch}}, N_m^{\text{arch}}$, and $N_{\text{tse}}^{\text{arch}}$ are the numbers of fixed, movable, and T-SE switching elements used in the switch *arch*, respectively.

We use a relative cost model to quantify and compare the cost of the proposed switch. We use the cost of the fixed elements C_f as a reference since the cost of these components is relatively stable compared to the other two types.

Let ρ be the ratio of the cost of movable versus fixed components, i.e., $\rho = C_m/C_f$. Similarly, let μ be the ratio of the cost of a T-SE versus a fixed component, i.e., $\mu = C_{\text{tse}}/C_f$. To evaluate the cost-effectiveness of the proposed switch as compared to an SaD-I switch, we use the total number of fixed and movable components in Table I to set up the following inequality:

$$N^2 C_m + N\Phi C_f \geq N^2 C_{\text{tse}}. \tag{9}$$

By simplifying inequality (9), it is straightforward to show that the proposed switch has a smaller overall cost as compared to that of SaD-I if and only if the value of σ satisfies the following inequality:

$$\rho_{\text{SaD-I}} \geq \mu - \frac{(2^{(\lceil \log_2(N) \rceil + 1)} - 2)}{N}. \tag{10}$$

Similarly, we can compute a lower bound on the value of ρ for the SaD-II and SUM-SaD as follows:

$$\rho_{\text{SaD-II}} \geq \frac{\mu N - 2^{\lceil \log_2(N) \rceil} - 1}{N + 3 \times 2^{\lceil \log_2(N) \rceil} - 3}, \tag{11}$$

$$\rho_{\text{SUM-SaD}} \geq \frac{\mu N - 2^{\lceil \log_2(N) \rceil} - 1}{2N}. \tag{12}$$

Figure 7 plots the ratio ρ/μ to provide an insight on the relationship between the cost of a T-SE and that of a movable component. Moreover, we plot the function $1/\mu$ (i.e., $\rho = 1$), which corresponds to the case $C_m = C_f$. Obviously, the cost of a MEMS mirror $C_m > C_f$. Therefore,

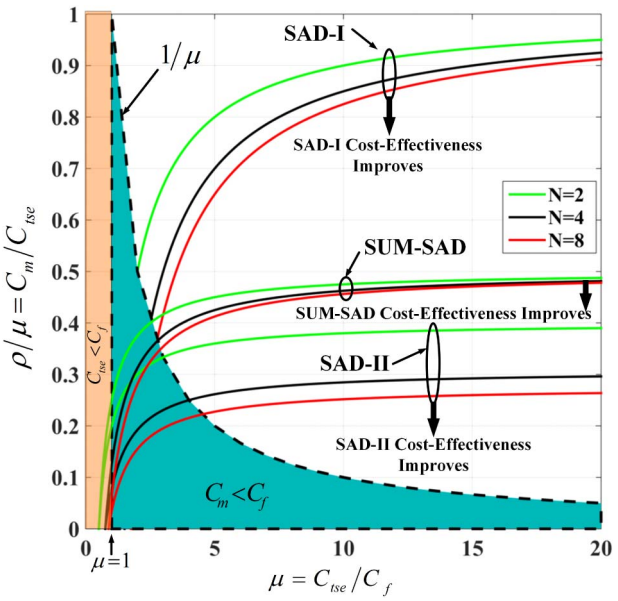

Fig. 7. Cost analysis of the proposed switch.

we consider the shaded area below the curve $1/\mu$ as an invalid design region. It is not expected that the cost C_{tse} will be less than C_f. Therefore, we have also excluded the area corresponding to $\mu < 1$.

Given the costs of various hardware components, one can use Fig. 7 to compare the cost-effectiveness of the proposed design with respect to SaD-based switches at different port sizes ($N = 4$, 8, 16, and 32). For $N = 4$, even if the cost of a T-SE is 10× the cost of fixed components (i.e., $C_{\text{tse}} = 10 \times C_f$), the proposed switch will be more cost-effective as compared to the SaD-I, SaD-II, and SUM-SaD when C_{tse} is at most 1.18, 3.5, and $2.16 \times C_m$, respectively.

V. Discussion on Switching Performance

In this section we investigate the scalability and the switching delay of the proposed switch.

A. Scalability

From the previous analysis, we identify two factors, in addition to Gaussian beam propagation loss, that impact the performance of the proposed multicast switch: the material imperfection of T-SE and the signal split within the crossbar switch.

Tri-state materials are still in their infancy, and hence, the values of the parameters of the commercial material used in our study are modest. We believe that, as the quality of the tri-state materials improve, so will the performance of the proposed switch.

The second factor that impacts the performance of the proposed switch is the cascaded splitting nature of signal power along the way from the input to the outputs. This splitting behavior results in higher power loss and unequal signal power at output ports. For example, to multicast a signal to four outputs, using a typical signal splitting process will result in 1/4 of the input power at each of the four outputs. In the used crossbar structure, the signal power at the last output will be 1/8 of the input power. We believe that this high splitting loss can be alleviated using better switch structures such as multistage switching networks, e.g., Beneš and Spanke-Beneš. Multistage structures can avoid the sequential splitting property of a typical crossbar switch.

B. Switching Delay

The switching latency of the T-SEs depends on the properties of its material. In the case of the e-TransFlector material, the switching delay ranges from 10 to 100 ms at 20°C [27]. In [28], the switching latency of a 12″ × 15″ switchable mirror (SM) based e-TransFlector and tuned for the IR spectrum is about 250 ms. The authors expect that, for a 1″ × 1″ SM, the switching latency will be around 20 ms since the switching latency is proportional to the surface area of the SM [28]. We envision that the dimensions of the T-SEs in the proposed switch are much smaller than 1″ × 1″; thus the switching delay can be reduced.

VI. Conclusion

We propose a new class of SNB FSO multicast switches using T-SEs. In the proposed switch, T-SEs simultaneously support signal splitting and switching without the need for separate splitting stages used in conventional multicast switches. Thus, a beam propagating in the proposed switch avoids the propagation loss that may be encountered by an optical beam passing through a splitting stage followed by a crossbar, as in SaD-based switches. This leads to lower insertion loss due to Gaussian beam divergence. An $N \times M$ SNB multicast switch requires *only NM nonmovable* T-SEs. Comparison with existing optical multicast switches shows that the proposed switch provides multicast capability with lower hardware complexity and a comparable performance. Cost analysis for the proposed switch shows that its cost is lower than SaD-based switches, even if the cost of the T-SE is 1.2 to 3.5× that of a MEMS mirror.

Appendix A: Proof of Theorem 1

Theorem 1. An $N \times N$ crossbar switch employing T-SEs is strictly a nonblocking multicast switch.

Proof: We will use induction to prove the theorem. It is clear that all permutations, multicast assignments, and broadcast connections can be realized for the 3×3 switch (i.e., $N = 3$), as shown in Fig. 8. For simplicity, we change the indexing of ports. This change does not affect the functionality or the performance of the switch in any way.

Assume that an $(N - 1) \times (N - 1)$ switch is strictly nonblocking. Hence, it is always possible to connect any idle

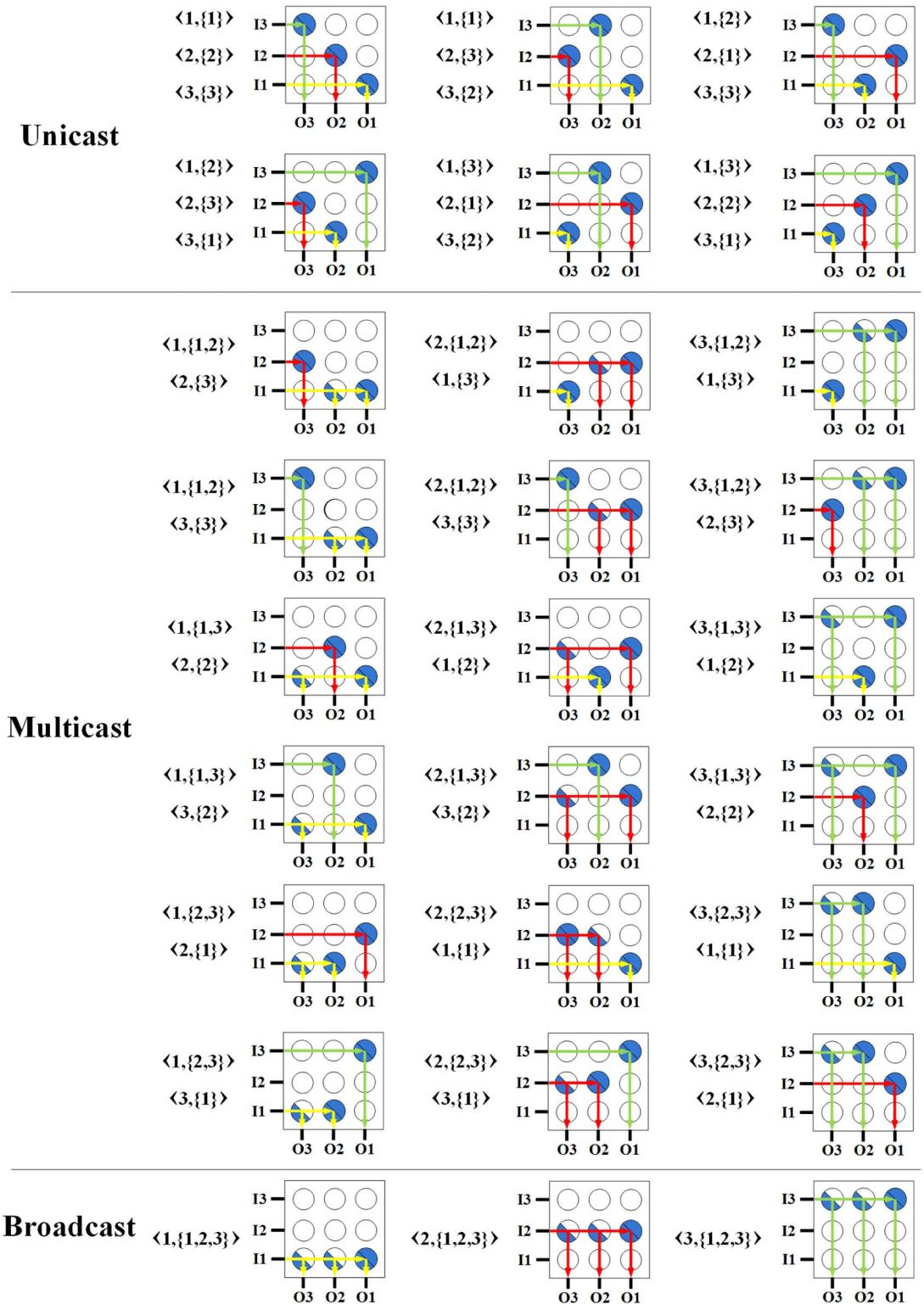

Fig. 8. Possible permutations using the proposed 3 × 3 switch.

input terminal to an arbitrary set of idle output terminals independent of the switch's current state. By induction, we wish to prove that an $N \times N$ switch is also strictly nonblocking.

For the induction step, an $N \times N$ switch can be obtained by adding a row and a column to the $(N-1) \times (N-1)$ switch, as shown in Fig. 9. The set of requests $\mathcal{R}^{N\times N}$ for an $N \times N$ switch can be defined as $\mathcal{R}^{N\times N} = \mathcal{R}^{(N-1)\times(N-1)} \cup \mathcal{R}_N$,

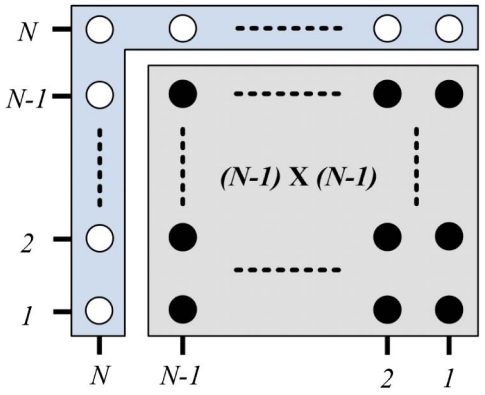

Fig. 9. $N \times N$ switch with an $(N-1) \times (N-1)$ sub-switch used in the induction step.

where $\mathcal{R}_N = \langle I_N, \Omega_N \rangle$. The added $2N-1$ T-SEs are configured in the T-state. This way, none of the $N-1$ inputs are affected, and therefore the functionality and the state of the $(N-1) \times (N-1)$ sub-switch is not affected. For the $N \times N$ switch to be strictly nonblocking, it is sufficient to show the following:

1) The input I_N can request any arbitrary set Ω_N of idle output terminals including the new Nth output port O_N without changing the states of any of the T-SEs of the $(N-1) \times (N-1)$ sub-switch.
2) The output O_N can be requested by any of the input ports including the new Nth input port I_N without changing the states of any of the T-SEs of the $(N-1) \times (N-1)$ sub-switch.

In general, for a request $\langle I_p, \Omega_p \rangle$, the switch is configured based on a descending order of ports in Ω_p. All possible scenarios can be summarized in the following four cases based on the status of $\mathcal{R}_N$ and O_N:

Case 1. $\Omega_N = \varnothing$, and $O_N \notin \Omega_i$, where $1 \le i \le |\mathcal{R}^{N \times N}|$.

The added row and column of T-SEs have no impact on the $(N-1) \times (N-1)$ sub-switch because $\Omega_N = \varnothing$ has not changed. Hence, the $N \times N$ switch is SNB.

Case 2. $\Omega_N \neq \varnothing$, and $O_N \notin \Omega_i$, where $1 \le i \le |\mathcal{R}^{N \times N}|$.

Let $\Omega_p = \{O^p_{q,k} | 1 \le q \le N, 1 < k \le |\Omega_p| \text{ and } \forall\, v, w \in k; O^p_{q,v} < O^p_{q,w} \text{ if } v < w\}$. The request $\mathcal{R}_p$ can be processed by configuring $\tau(p,j,\chi), \forall\, O^p_{j,k} \in \Omega_p$, as follows:

$$\tau(p,j,\chi) = \begin{cases} \tau(p,j,S), & \text{if } 1 \le k \le |\Omega_p| - 1 \\ \tau(p,j,R), & \text{if } k = |\Omega_p| \end{cases}. \tag{A1}$$

In this case, the request $\mathcal{R}_N$ can be processed by configuring $\tau(N,j,\chi), \forall\, O^N_{j,k} \in \Omega_N$, as follows:

$$\tau(N,j,\chi) = \begin{cases} \tau(N,j,S), & \text{if } 1 \le k \le |\Omega_N| - 1 \\ \tau(N,j,R), & \text{if } k = |\Omega_N| \end{cases}. \tag{A2}$$

It is easy to see that an idle output in the $(N-1) \times (N-1)$ sub-switch indicates that all the T-SEs in its column are in the T-state. Therefore, no states need to be changed in the $(N-1) \times (N-1)$ sub-switch. It follows that the $N \times N$ switch is SNB.

Case 3. $O_N \in \Omega_N$.

This case follows the analysis in Case 2 except that Ω_N has at least one output (i.e., O_N). From Eq. (A2), if the request is unicast, then $\mathrm{SE}(N,N)$ is configured in the R-state [i.e., $\tau(N,N,R)$]. If there are other output ports in Ω_N, then we will have $\tau(N,N,S)$, $\tau(N,j,S)$ for $2 \le k \le |\Omega_p| - 1$ and $\tau(N,j,R)$ for $k = |\Omega_p|$.

Case 4. $O_N \in \Omega_x$, where $x \neq N$ and $\mathcal{R}_x \in \mathcal{R}^{(N-1)\times(N-1)}$.

The request $\mathcal{R}_N$ can be realized using the same argument as in Case 2. If $\mathcal{R}_x \in \Gamma$, then this can be easily realized by configuring $\tau(x,N,R)$, making the $N \times N$ switch SNB. On the other hand, if $\mathcal{R}_x \in \Psi$, the request can be realized by configuring $\tau(x,N,S)$, where the input signal I_x is split at $\tau(x,N,S)$. Accordingly, one part of the signal goes to the output port O_N, whereas the other part goes to the $(N-1) \times (N-1)$ sub-switch. The $(N-1) \times (N-1)$ sub-switch is assumed to be SNB, and therefore the $N \times N$ switch is SNB. ∎

References

[1] Z. Cao, R. Proietti, and S. J. B. Yoo, "Hi-LION: Hierarchical large-scale interconnection optical network with AWGRs [Invited]," *J. Opt. Commun. Netw.*, vol. 7, no. 1, pp. A97–A105, Jan. 2015.

[2] A. Hamza, J. Deogun, and D. Alexander, "Free space optical data center architecture design with fully connected racks," in *IEEE Global Communications Conf.*, Dec. 2014, pp. 2192–2197.

[3] A. S. Hamza, J. S. Deogun, and D. Alexander, "Evolution of data centers: A critical analysis of standards and challenges for FSO links," in *IEEE Conf. on Standards for Communications and Networking (CSCN)*, Oct. 2015, pp. 100–105.

[4] Z. Zhu, S. Zhong, L. Chen, and K. Chen, "Fully programmable and scalable optical switching fabric for petabyte data center," *Opt. Express*, vol. 23, no. 3, pp. 3563–3580, Feb. 2015.

[5] G. Wang, D. G. Andersen, M. Kaminsky, K. Papagiannaki, T. E. Ng, M. Kozuch, and M. Ryan, "c-Through: Part-time optics in data centers," *ACM SIGCOMM Comput. Commun. Rev.*, vol. 40, no. 4, pp. 327–338, 2010.

[6] K. Chen, A. Singla, A. Singh, K. Ramachandran, L. Xu, Y. Zhang, X. Wen, and Y. Chen, "OSA: An optical switching architecture for data center networks with unprecedented flexibility," *IEEE/ACM Trans. Netw.*, vol. 22, no. 2, pp. 498–511, Apr. 2014.

[7] K. Christodoulopoulos, D. Lugones, K. Katrinis, M. Ruffini, and D. O'Mahony, "Performance evaluation of a hybrid optical/electrical interconnect," *J. Opt. Commun. Netw.*, vol. 7, no. 3, pp. 193–204, Mar. 2015.

[8] O. Liboiron-Ladouceur, I. Cerutti, P. G. Raponi, N. Andriolli, and P. Castoldi, "Energy-efficient design of a scalable optical multiplane interconnection architecture," *IEEE J. Sel. Top. Quantum Electron.*, vol. 17, no. 2, pp. 377–383, Mar. 2011.

[9] M. Fiorani, M. Casoni, and S. Aleksic, "Performance and power consumption analysis of a hybrid optical core node," *J. Opt. Commun. Netw.*, vol. 3, no. 6, pp. 502–513, 2011.

[10] Y. Yin, R. Proietti, X. Ye, C. Nitta, V. Akella, and S. Yoo, "LIONS: An AWGR-based low-latency optical switch for

high-performance computing and data centers," *IEEE J. Sel. Top. Quantum Electron.*, vol. 19, no. 2, 3600409, Mar. 2013.

[11] M. Fiorani, S. Aleksic, P. Monti, J. Chen, M. Casoni, and L. Wosinska, "Energy efficiency of an integrated intra-data-center and core network with edge caching," *J. Opt. Commun. Netw.*, vol. 6, no. 4, pp. 421–432, 2014.

[12] R. Proietti, Z. Cao, C. Nitta, Y. Li, and S. Yoo, "A scalable, low-latency, high-throughput, optical interconnect architecture based on arrayed waveguide grating routers," *J. Lightwave Technol.*, vol. 33, no. 4, pp. 911–920, 2015.

[13] C. Zhang and W. Hu, "Design and analysis of a multicast-capable optical cross-connect," *Proc. SPIE*, vol. 7136, 71364H, 2008.

[14] H. Du, W. Hu, H. He, C. Zhang, Y. Dong, W. Sun, W. Guo, Y. Jin, and S. Xiao, "Separated unicast/multicast splitter-and-delivery switch and its use in multicasting-capable optical cross-connect," *IEEE Photon. Technol. Lett.*, vol. 21, no. 6, pp. 368–370, 2009.

[15] S. Chua and B. Li, *Optical Switches: Materials and Design*, Woodhead Publishing Series in Electronic and Optical Materials. Elsevier, 2010.

[16] M. Imran, M. Collier, P. Landais, and K. Katrinis, "HOSA: Hybrid optical switch architecture for data center networks," in *ACM Int. Conf. on Computing Frontiers*, New York, 2015, article 27.

[17] G. Baxter, S. Frisken, D. Abakoumov, H. Zhou, I. Clarke, A. Bartos, and S. Poole, "Highly programmable wavelength selective switch based on liquid crystal on silicon switching elements," in *Optical Fiber Communication Conf. (OFC)*, Mar. 2006, pp. 1–3.

[18] T. Benson, A. Akella, and D. A. Maltz, "Network traffic characteristics of data centers in the wild," in *Proc. 10th ACM SIGCOMM Conf. on Internet Measurement*, New York, 2010, pp. 267–280.

[19] M. Imran, P. Landais, M. Collier, and K. Katrinis, "Performance analysis of optical burst switching with fast optical switches for data center networks," in *Int. Conf. on Transparent Optical Networks*, Budapest, Hungary, 2015, pp. 1–4.

[20] W. Hu and Q. Zeng, "Multicasting optical cross connects employing splitter-and-delivery switch," *IEEE Photon. Technol. Lett.*, vol. 10, no. 7, pp. 970–972, 1998.

[21] Y. Xin and G. Rouskas, "Multicast routing under optical layer constraints," in *INFOCOM*, 2004, vol. 4, pp. 2731–2742.

[22] L. Y. Lin, E. L. Goldstein, and R. W. Tkach, "Free-space micromachined optical switches for optical networking," *IEEE J. Sel. Top. Quantum Electron.*, vol. 5, no. 1, pp. 4–9, 1999.

[23] A. S. Hamza, J. Deogun, and D. Alexander, "Free space optical multicast crossbar switch with non-movable switching elements," in *Advanced Photonics for Communications*, 2014, paper JT3A.13.

[24] A. S. Hamza, J. S. Deogun, and D. Alexander, "Rearrangeable non-blocking multicast FSO switch using fixed switching elements," in *IEEE Global Communications Conf.*, to be published.

[25] L.-Y. Lin, E. Goldstein, and R. Tkach, "On the expandability of free-space micromachined optical cross connects," *J. Lightwave Technol.*, vol. 18, no. 4, pp. 482–489, 2000.

[26] C. Li, G. Li, V. Li, P. Wai, H. Xie, and X. Yuan, "Using 2×2 switching modules to build large 2-D MEMS optical switches," in *IEEE Global Communications Conf.*, Dec. 2003, vol. 5, pp. 2798–2802.

[27] "Switchable mirrors/switchable glass," Kent Optronics, 2012. [Online]. Available: http://kentoptronics.com/switchable.html.

[28] N. Hamedazimi, Z. Qazi, H. Gupta, V. Sekar, S. R. Das, J. P. Longtin, H. Shah, and A. Tanwer, "Firefly: A reconfigurable wireless data center fabric using free-space optics," in *ACM SIGCOMM*, 2014, pp. 319–330.

[29] O. Solgaard, *Photonic Microsystems: Micro and Nanotechnology Applied to Optical Devices and Systems*, MEMS Reference Shelf. Springer, 2009.

[30] G. Shen, T. H. Cheng, S. K. Bose, C. Lu, and T. Y. Chai, "A novel rearrangeable non-blocking architecture for MEMS optical space switch," *Opt. Netw. Mag.*, vol. 3, no. 6, pp. 70–79, 2002.

[31] V. Li, C. Y. Li, and P. K. A. Wai, "Alternative structures for two-dimensional MEMS optical switches [Invited]," *J. Opt. Netw.*, vol. 3, no. 10, pp. 742–757, Oct. 2004.

[32] K. Murata, T. Saida, K. Sano, I. Ogawa, H. Fukuyama, R. Kasahara, Y. Muramoto, H. Nosaka, S. Tsunashima, T. Mizuno, H. Tanobe, K. Hattori, T. Yoshimatsu, H. Kawakami, and E. Yoshida, "100-gbit/s PDM-QPSK coherent receiver with wide dynamic range and excellent common-mode rejection ratio," *Opt. Express*, vol. 19, no. 26, pp. B125–B130, Dec. 2011.